RSC Chemical Biology

ROYAL SOCIETY OF CHEMISTRY

PAPER

View Article Online
View Journal | View Issue



Cite this: *RSC Chem. Biol.*, 2022, 3, 85

# A ruthenium–oligonucleotide bioconjugated photosensitizing aptamer for cancer cell specific photodynamic therapy†

Luke K. McKenzie, ‡[ab] Marie Flamme, ‡[abc] Patrick S. Felder, [b] Johannes Karges, [b] Frederic Bonhomme, [d] Albert Gandioso, [b] Christian Malosse,[e] Gilles Gasser *[b] and Marcel Hollenstein *[a]

Received 13th July 2021,
Accepted 31st October 2021

DOI: 10.1039/d1cb00146a

rsc.li/rsc-chembio

Ruthenium complexes have emerged as a promising class of compounds for use as photosensitizers (PSs) in photodynamic therapy (PDT) due to their attractive photophysical properties and relative ease of chemical alteration. While promising, they generally are not inherently targeting to disease sites and may therefore be prone to side effects and require higher doses. Aptamers are short oligonucleotides that bind specific targets with high affinity. One such aptamer is **AS1411**, a nucleolin targeting, G-quadruplex forming, DNA aptamer. Here we present the first example of direct conjugation of a Ru(II) polypyridyl complex-based PS to an aptamer and an assessment of its *in vitro* cancer cell specific photosensitization including discussion of the challenges faced.

## Introduction

The exploration of ruthenium (Ru) complexes for use as photosensitizers (PSs) for photodynamic therapy (PDT) has exploded in recent years[1–13] and, with the recent entrance into clinical trials of the Ru(II)-based PS **TLD-1433**, this looks only likely to intensify.[7] PDT combines a PS, activating light and cellular oxygen to produce $^1O_2$/reactive oxygen species (ROS) resulting in localised cell death.[3] While PDT of cancer promises tumour specificity through localised irradiation at the tumour site, the PS has generally only a low cancer cell specificity. A number of strategies have been investigated to enhance the cancer specificity and/or organelle specific targeting of Ru-based PDT PSs such as bioconjugation to proteins[11,14–16] and nanobodies[17] as well as through nanoparticle incorporation.[18–22] This would allow for the use of lower doses of PS and the reduction of side effects.

One targeting modality, little explored in combination with ruthenium complexes, is the use of aptamers.[23] Aptamers are short oligonucleotides with high binding affinity to a specific target, such as proteins or entire cells, and are usually selected through the Systematic Evolution of Ligands by Exponential enrichment (SELEX) process.[24–26] Aptamers are considered to be nucleic acid analogues of antibodies but offer a number of advantages such as synthetic reproducibility and comparatively low-cost, high scale, synthesis. One such aptamer is **AS1411**, unusually discovered accidentally rather than through the traditional SELEX process.[27] **AS1411** is an aptamer for nucleolin, a protein generally expressed in the nucleoli of cells, though overexpressed in a wide number of cancer cell lines with atypical cell surface expression.[28] **AS1411** has been shown to be internalised in many cancer cells lines such as breast (MCF7) and prostate (DU145), among many others, while normal cell lines typically do not incorporate the aptamer.[29] The G-rich oligonucleotide forms a G-quadruplex in the presence of certain metal ions such as $K^+$ and this formation is believed to be required for uptake. **AS1411** has been explored as a potential cancer specific drug delivery system with drug loading *via* intercalation[30] as well as through covalent linking.[31,32] Kim *et al.* recently conjugated the known PS **Ce6** to the 3′-end of **AS1411** *via* a PEG chain. Photosensitization in the nanomolar range was observed for the resulting aptamer in three cancer cell

[a] *Institut Pasteur, Department of Structural Biology and Chemistry, Laboratory for Bioorganic Chemistry of Nucleic Acids, CNRS UMR3523, 28 rue du Docteur Roux, 75724 Paris Cedex 15, France. E-mail: marcel.hollenstein@pasteur.fr; Web: https://research.pasteur.fr/en/team/bioorganic-chemistry-of-nucleic-acids/; Tel: +33 1 44 38 94 66*

[b] *Chimie ParisTech, PSL University, CNRS, Institute of Chemistry for Life and Health Sciences, Laboratory for Inorganic Chemical Biology, 75005 Paris, France. E-mail: gilles.gasser@chimieparistech.psl.eu; Web: www.gassergroup.com; Tel: +33 1 85 78 41 51*

[c] *Université de Paris, 12 rue de l'École de Médecine, 75006 Paris, France*

[d] *Institut Pasteur, Department of Structural Biology and Chemistry, Unité de Chimie Biologique Epigénétique, UMR CNRS 3523, 28 rue du Docteur Roux, 75724 Paris Cedex 15, France*

[e] *Institut Pasteur, Mass Spectrometry for Biology Unit, 28 rue du Docteur Roux, 75724 Paris Cedex 15, France*

† Electronic supplementary information (ESI) available. See DOI: 10.1039/d1cb00146a

‡ Authors contributed equally.

lines (MCF-7, HCT 116, and SKOV-3) while no photosensitization was observed in a normal cell line (L-929).[33] A number of papers have been released exploring the use of **AS1411** for targeted PDT including both direct conjugation[33,34] and intercalation.[30] Previously, the ruthenium complex $[Ru(bpy)_2(tip)]^{2+}$ was loaded into nanoparticles adorned with **AS1411** for cell specific release with the system improving survival in a murine glioma model.[35] The direct use of Ruthenium complexes with **AS1411** in this context poses some previously unexplored questions. Certain ruthenium complexes are known to interact with G-quadruplexes, for example a series of dinuclear Ruthenium complexes were shown to bind to and stabilise telomeric G-quadruplexes.[36] While many Ruthenium complexes have been demonstrated to specifically target, and usually stabilize, G-quadruplex DNA over standard DNA duplexes.[36–44] As such we faced the question of whether to approach the system *via* intercalation, as demonstrated previously with the non-ruthenium PS **TMPyP**[30] or by conjugation, eventually settling with the latter due to questions of complete intercalation would be achieved and whether intercalation may result in quenching and reduction of $^1O_2$ yields.

We recently published our findings of a series of rationally designed Ru(II) polypyridine complexes based on the $[Ru(phen)_2(bpy)]^{2+}$ scaffold of which one complex (**Ru**) was demonstrated to be capable of remarkable photosensitization in the nanomolar range at 595 nm (Fig. 1a).[1] Capitalizing on the excellent results obtained by Kim *et al.*, we decided to investigate whether the coupling of **Ru** to this aptamer would indeed allow for selective targeting of cancer cells. Through addition of azide functionality the resulting complex (**$RuN_3$**) may be suitable for use in a diverse range of applications beyond those explored in this study such as dye sensitized solar cells (DSSCs) and catalysis.[45] In this article, we describe the design, synthesis, biophysical characterization, and *in vitro* evaluation of a series of ruthenium–**AS1411** conjugates (**Ru–AS1411**) utilizing **Ru** in combination with the cancer-targeting aptamer **AS1411**.[1]

# Results and discussion

### Synthesis and characterisation

The previously reported **Ru** (Fig. 1a) was chosen for conjugation to **AS1411** due to its remarkable photophysical and photosensitizing properties at wavelengths up to 595 nm.[1]

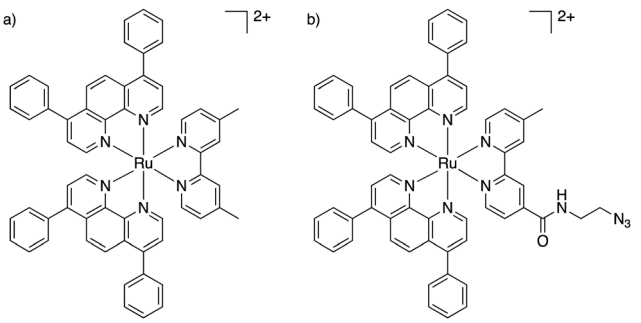


Fig. 1 Chemical structures of (a) **Ru**;[1] (b) **$RuN_3$**.

Through the addition of an azide functionality on the bipyridine ligand, the resulting Ru(II) complex (**$RuN_3$**) (Fig. 1b) is primed to form the ruthenium-containing aptamer conjugates (**Ru–AS1411s**, Fig. S1, ESI†) through the standard Cu(I)-catalyzed azide–alkyne cycloaddition (click) reaction. The **AS1411** aptamer consists of a 26 mer sequence (template **T1**, Table 1). With the rationale of reduced G-quadruplex disruption, three spacer Ts were appended at the 3′-end followed by 3′ alkyne modification resulting in the 29 mer sequence **T2** (Table 1). We also designed sequences **T3** and **T4** where the alkyne moiety is placed at the 5′ rather than at the 3′ position of **AS1411** aptamer to probe the effect on PDT efficiency and G-quadruplex formation capacity and with shorter (**T3**) and longer (**T4**) connecting linker moieties.

### $RuN_3$ synthesis

The synthesis of **$RuN_3$** was achieved by adapting previously published procedures.[46–51] The synthesis of **$[RuBphen_2Cl_2]$** was found to be more efficient *via* the intermediate **$[Ru(dmso)_4Cl_2]$** (Fig. 2) than by direct synthesis from commercially available $RuCl_3$, a finding that has been hinted at in the literature.[46] LiCl is used as an additive during the synthesis of **$[RuBphen_2Cl_2]$** to prevent the formation of the tri-substituted **$[Ru(Bphen)_3]Cl_2$** as an undesired side product (**Bphen** = 4,7-diphenyl-1,10-phenanthroline, also known as bathophenanthroline). The synthesis of **$bpyN_3$** was performed *via* EDCI-based amide coupling. 4′-Methyl-[2,2′-bipyridine]-4-carboxylic acid is commercially available while 2-azidoethan-1-amine (**$N_3EtNH_2$**) was produced by nucleophilic substitution of 2-chloroethylamine with sodium azide.[52] The ligand **$bpyN_3$** was directly coordinated to the Ru(II) precursor **$[RuBphen_2Cl_2]$** to obtain **$RuN_3$**.

**$RuN_3$** was fully characterized by NMR (Fig. S3–S8, ESI†), HR-MS ESI (Fig. S9, ESI†) and IR spectroscopy (Fig. S10, ESI†). Present are the characteristic patterns of the disubstituted phen and bpy ligands (8.0–9.0 ppm), as well as the rotating phen groups (7.5 ppm, broad), the four protons of the aliphatic $EtN_3$ end (3.5–3.6 ppm) and the three methyl protons (2.6 ppm), the structure was successfully identified by $^1$H NMR (Fig. S3, ESI†). The molecular formula of **$RuN_3$** was confirmed by HR-MS ($C_{62}H_{46}N_{10}ORu$, expected: 524.1453, found: 524.1447) in positive mode as the $[M]^{2+}$ ion (Fig. S9, ESI†). The characteristic azide peak in the IR spectrum was identified at 2100 $cm^{-1}$, interestingly, it was observed that the IR spectrum is strongly dominated by the large amount of delocalized C–C signal (Fig. S10, ESI†).

Table 1 Sequences of the oligonucleotides used. Structure of alkyne[1] and alkyne[2] can be found in Fig. S2

| Oligonucleotide | Sequence |
|---|---|
| **T1** | 5′-GGT GGT GGT GGT TGT GGT GGT GGT GG-3′ |
| **T2** | 5′-GGT GGT GGT GGT TGT GGT GGT GGT GGT TT-alkyne[1]-3′ |
| **T3** | 5′-alkyne[2]-TTG GTG GTG GTG GTT GTG GTG GTG GTG G-3′ |
| **T4** | 5′-alkyne[2]-TTT TTG GTG GTG GTG GTT GTG GTG GTG GTG G-3′ |
| **T5** | 5′-FAM-GGT GGT GGT GGT TGT GGT GGT GGT GG-3′ |

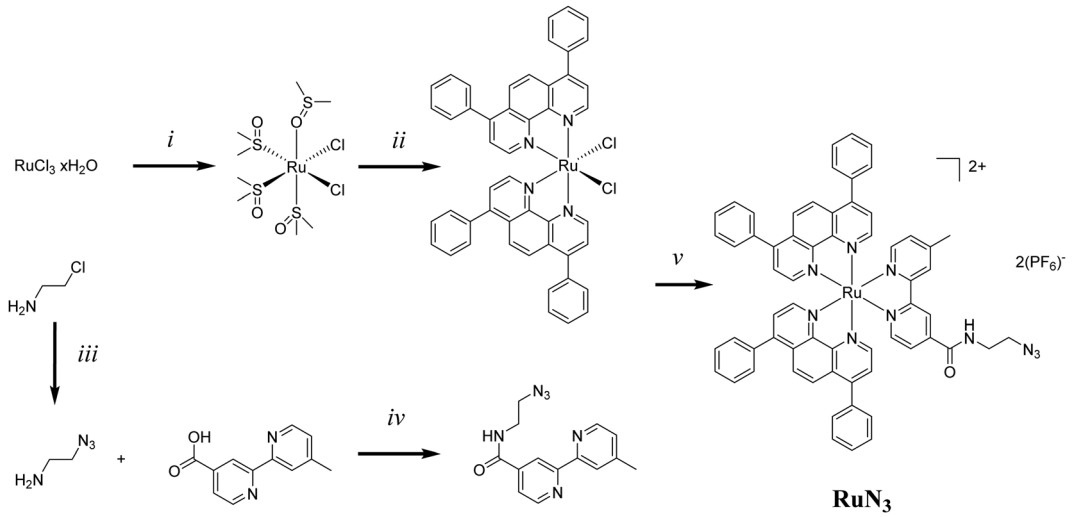


Fig. 2 Synthetic procedure for **RuN$_3$**; (i) EtOH DMSO, reflux, 4 h; DMSO, 125 °C, 1 h, 85%; (ii) Bphen, LiCl, DMF, reflux, 5 h, 72%; (iii) $NaN_3$, $H_2O$, 80 °C, 12 h, 82%; (iv) EDCI, NHS, DIPEA, $CH_2Cl_2$, r.t., 12 h, 56%; (v) MeOH, $H_2O$, reflux, 15 h, 64%.

### RuN$_3$ Photophysical and biological analyses

The absorption spectrum of **RuN$_3$** (Fig. S11a, ESI†) exhibits the two Soret bands typical for this type of Bphen-containing Ru(II) complex.[4,49,53–55] The local maximum at 470 nm, with bathochromic off-tailing up to 600 nm,[49,54] is associated with the PDT-active metal-to-ligand charge transfer (MLCT) band. **RuN$_3$** has a large Stokes shift (0.74 eV) with an emission maximum at 640 nm (in acetonitrile, Fig. S11b, ESI†) and a luminescence quantum yield of $\Phi$ = 2.6% in comparison to $[Ru(bpy)_3]Cl_2$ ($\Phi$ = 5.9%).[56] The excited state lifetime was determined to be 220 ns in an air-saturated and 1076 ns in a degassed environment, which is comparable with $[Ru(bpy)_3]Cl_2$.[2,49,54] The change of the excited state lifetime is indicative of an interaction of the metal complex with molecular oxygen. The singlet oxygen yield ($\Phi\Delta$) of **RuN$_3$** was measured by both direct measurement of singlet oxygen phosphorescence and by indirect measurement using $^1O_2$ scavengers as previously described.[57] **RuN$_3$** was found with a value of 68% using the direct method ($\lambda_{exc}$ = 450 nm, acetonitrile), similarly to **Ru** under the same conditions (61%[1]). The $\Phi\Delta$ upon excitation at 595 nm was still impressive (51% in acetonitrile, Table 2) indicating suitability for use as a PS over a range of activation wavelengths.

Next, **RuN$_3$** was tested in MCF-7 (breast cancer) and RPE-1 (normal retina) cell lines to determine its light and dark toxicities with irradiation at 480 nm (10 min, 3.21 J cm$^{-2}$) and 595 nm (2 h, 22.47 J cm$^{-2}$) (Table 3). The results indicate that addition of the linker does not hinder the photosensitizing action of **RuN$_3$** while addition of the azide linker appears to generally reduce the dark toxicity of the molecule compared to **Ru**.[1]

### Ru–AS1411 conjugates

Click reactions were chosen for conjugation due to perceived ease and accessibility.[58–60] We initially followed the reaction conditions set out in a paper describing the ideal click conditions for use with oligonucleotides.[61] The initial click reactions were between **RuN$_3$** and **T2** aiming to yield the system **AS1411-3′-TTT-Ru**. To avoid intercalation of **RuN$_3$** during the reaction the phosphate-buffered saline (PBS) in the published protocol was replaced with tris-buffered saline to avoid $K^+$ and hence G-quadruplex formation. Similarly, the 'Monarch® PCR & DNA Cleanup Kit' was chosen for desalting the sample prior to HPLC purification as the binding buffer does not contain potassium. While PAGE of the click product confirmed conjugation (Fig. S12, ESI†), no G-quadruplex formation was observed by CD spectroscopy (Fig. S13a, ESI†). G-quadruplexes are known to produce distinctive peaks in their CD spectra when formed, as seen for **AS1411** (Fig. S13b, ESI†), and CD spectroscopy is used as a means to validate their presence.[62–64] In the case of **AS1411**, the distinctive CD signature includes a positive peak at around 260 nm and a negative peak at around 240 nm[63,65] which were not observed when **Ru** was attached at the 3′ end under these experimental conditions regardless on the concentration of $K^+$. Nevertheless, an *in vitro* PDT assay was performed using MCF-7 (breast cancer), HT-29 (colorectal adenocarcinoma) and RPE-1 (retinal pigment epithelial) cell lines. MCF-7 cells are cell surface

Table 2 Spectroscopic properties and singlet oxygen yield measurements for **RuN$_3$**; (a) acetonitrile; (b) PBS

| | Spectroscopic properties | | | | | Singlet oxygen yield (%) | | | |
|---|---|---|---|---|---|---|---|---|---|
| | UV/vis absorption $\lambda$, nm ($\varepsilon$, M$^{-1}$ cm$^{-1}$ × 10$^3$) | $\lambda_{em}$ (nm) | $\Phi_{em}$ (%) | $\tau$ air saturated (μs) | $\tau$ degassed (μs) | 450 nm direct | 450 nm indirect | 540 nm indirect | 595 nm indirect |
| **RuN$_3$** | 278[a] (176); 433[a] (40); 463[a] (45) | 640[a] | 2.6[a] | 0.220[a] | 1.076[a] | 68[a] | 71[a], 7[b] | 64[a], 5[b] | 51[a], 3[b] |

Table 3 $LD_{50}$ values (μM) for **$RuN_3$** in the light 480 nm (10 min, 3.21 J $cm^{-2}$) or 595 nm (2 h, 22.47 J $cm^{-2}$) and dark in MCF-7 and RPE-1 cell lines

| | **$RuN_3$** | | | | | |
|---|---|---|---|---|---|---|
| | 480 nm | | | 595 nm | | |
| | Light | Dark | PI | Light | Dark | PI |
| MCF-7 | 0.574 (±0.060) | >100 | >174 | 2.081 (±0.050) | >100 | >48.05 |
| RPE-1 | 0.015 (±0.069) | 58.58 (±0.086) | 3905 | 0.946 (±0.150) | 69.31 (±0.166) | 73.3 |

nucleolin expressing cells and are widely used in *in vitro* tests of **AS1411**. An immunofluorescence assay confirmed cell surface nucleolin expression in HT-29 while no cell surface nucleolin expression was detected in RPE-1 cells (Fig. S14, ESI†). No PDT effect was observed following light treatment at 480 nm in any cell line up to 2 μM (data not included).

We hypothesised that this inability to form G-quadruplexes was either due to the position of the conjugated **Ru** or due to guanine oxidation issues arising from the click reaction.[66,67] In order to investigate the **Ru** hypothesis, we decided to conjugate the **Ru** at the 5′ end with both a two T or five T spacers **T3** and **T4**.

For the click reaction conditions in the outlined protocol,[61] 10 molar equivalents of $CuSO_4$ and 50 molar equivalents of sodium ascorbate are used in thoroughly degassed solution. To investigate the effect of these click conditions on G-quadruplex formation, **T2** alone (without **$RuN_3$**) was incubated under the same conditions. Post purification no G-quadruplex melting curve was detectable, indicating potential oxidation of guanine and loss of G-quadruplex formation (Fig. S15a, ESI†). **T2** was subsequently incubated with one molar equivalent of $CuSO_4$ and two molar equivalents of TBTA for 1, 2 and 18 hours with no loss of G-quadruplex melting curve (Fig. S15a, ESI†). Considering the complication encountered using click reactions in the context of conjugation of Ru(II) complexes to G-quadruplex-forming systems, we would advise the use of alternative coupling methods, or at least careful consideration of the click conditions prior to use.

The revised click conditions were used with **$RuN_3$** and **T3**, **T4** and **T2** to yield **AS1411-5′-TT-Ru**, **AS1411-5′-TTTTT-Ru** and **AS1411-3′-TTT-Ru** as monitored and purified by HPLC with confirmation of product formation by LCMS (Fig. S16, ESI†). G-quadruplex formation was confirmed for all three samples by CD spectroscopy (Fig. S17, ESI†), thermal difference spectra (TDS) (Fig. S18, ESI†) and $T_m$-melting experiments (Fig. S15b, ESI†). TDS spectra can be used to analyse types of G-quadruplex formed.[65] **AS1411-5′-TT-Ru**, **AS1411-5′-TTTTT-Ru** and **AS1411-3′-TTT-Ru** have $T_m$ values of 54.6, 51.5 and 61.6 °C respectively, measured in 0.1 M KCl, compared to 50.0 °C for unmodified **AS1411** (**T1**). It is interesting to note that position of the **Ru** relative to the **AS1411** core sequence has quite profound effects in the resulting $T_m$ values with a very large increase of 11.6 °C for conjugation at the 3′-end. This perhaps indicates formation of different G-quadruplex structures or the predominance of one particular structures of the at least 8 different monomeric structures[63] known to constitute **AS1411**. Hence, conjugation of **Ru** or possibly other substituents might represent a means to modulate the amount and the nature of G-quadruplex structures adopted by **AS1411**.

All three **Ru–AS1411** are prone to forming insoluble 'crystals' if dried to completion by speed vac. We hypothesise that this is due to intrastrand interactions whereby G-quadruplex formation is initiated by the conjugated ruthenium complexes. Partial solubility can be recovered by heating to 95 °C in a 100 mM KCl solution with vigorous shaking.

## Biological evaluation

All three **Ru–AS1411** were tested in MCF-7 (breast cancer) and RPE-1 (normal retina) cell lines as model cell surface nucleolin positive and negative cell lines. It is clear from the CD spectrum of **AS1411** that the cation concentration in the cell media used (5 mM KCl, 154 mM NaCl (DMEM)) is insufficient for complete G-quadruplex formation (Fig. S13b, ESI†). As such all **Ru–AS1411** were kept in stock solutions at 20 μM in 50 mM KCl. The additional KCl was kept constant across all wells including control wells. Following a 2 hour incubation and light treatment ($\lambda_{exc}$ = 480 nm, 3.21 J $cm^{-2}$, 10 min) **AS1411-5′-TTTTT-Ru** reduced cell viability to a greater extent in MCF7 cells compared to RPE-1 cells, demonstrating the potential for cell specific PDT (Table 4 and Fig. 3, Fig. S20a, ESI†). Interestingly **AS1411-5′-TTTTT-Ru** has a G-quadruplex $T_m$ closest to the original sequence (51.5 °C *vs.* 50.0 °C) perhaps suggesting that **AS1411-5′-TTTTT-Ru** maintains the same form of G-quadruplex. Confocal microscopy confirmed uptake in MCF7 and RPE-1 cells (Fig. S19, ESI†).[68] After a 4 hour incubation and light treatment

Table 4 $LD_{50}$ Values (μM) for **Ru–AS1411s** in the light 480 nm (10 min, 3.21 J $cm^{-2}$), 540 nm (40 min, 9.5 J $cm^{-2}$), 595 nm (2 h, 22.47 J $cm^{-2}$) and dark in MCF-7 and RPE-1 cell lines

| | **AS1411-5′-TTTTT-Ru** | | | | | | | **AS1411-5′-TT-Ru** | | | **AS1411-3′-TTT-Ru** | | |
|---|---|---|---|---|---|---|---|---|---|---|---|---|---|
| | 480 nm | | | 540 nm | | 595 nm | | 480 nm | | | 480 nm | | |
| | Light | Dark | PI | Light | Dark | Light | Dark | Light | Dark | PI | Light | Dark | PI |
| MCF-7 2 h | 0.340 (±0.077) | >1 | >2.9 | 0.990 (±0.061) | >1 | >1 | >1 | 0.524 (±0.070) | >1 | >1.9 | 0.370 (±0.084) | >1 | >2.7 |
| RPE-1 2 h | 0.735 (±0.084) | >1 | >1.36 | >1 | >1 | >1 | >1 | 0.582 (±0.065) | >1 | >1.7 | 0.474 (±0.084) | >1 | >2.1 |
| MCF-7 4 h | 0.120 (±0.043) | >1 | >8.33 | nd | nd | nd | nd | 0.274 (±0.032) | >1 | >3.6 | 0.134 (±0.032) | >1 | >7.5 |
| RPE-1 4 h | 0.082 (±0.058) | >1 | >12.19 | nd | nd | nd | nd | 0.231 (±0.047) | >1 | >4.3 | 0.181 (±0.059) | >1 | >5.5 |

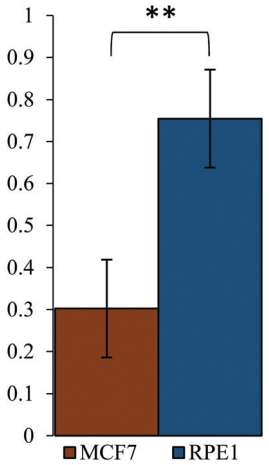


Fig. 3 Relative cell survival in MCF-7 and RPE1 cell lines following treatment with **AS1411-5′-TTTTT-Ru** (0.5 μM, 2 hours) and light (480 nm, 10 min, 3.21 J $cm^{-2}$). Significance evaluated by Student's *T*-Test ** $p < 0.01$.

($\lambda_{exc}$ = 480 nm, 3.21 J $cm^{-2}$, 10 min) all three **Ru–AS1411s** are phototoxic and cell line specificity is lost while only a mild reduction in cell viability is seen in the dark (Table 4 and Fig. S20b, ESI†). **$RuN_3$** alone is highly phototoxic after a 4 hour incubation in both cell lines (Table 3). Following a 2 hour incubation and light irradiation at 540 nm (40 min, 9.5 J $cm^{-2}$), **AS1411-5′-TTTTT-Ru** maintains phototoxicity in MCF-7 cells though at 595 nm (2 h, 22.47 J $cm^{-2}$) we were unable to detect phototoxicity within our concentration range (up to 1 μM). We believe this is due to the low range of concentrations tested coupled with the longer irradiation times.

It was hypothesized that loss of specificity at 4 hours may be due to nuclease-mediated degradation of the oligonucleotides in cell media. As such a stability test was performed in cell medium (DMEM, 10% Foetal calf serum) to investigate the degradation, if any, of the oligonucleotides (Fig. S21, ESI†). It is clear that **AS1411** alone (with 5′-FAM, **T5**) is susceptible to degradation with a significant laddering in the PAGE gel from the 30 minute incubation. Where Ru conjugation is at the 3′ end, in **AS1411-3′-TTT-Ru**, degradation appears lessen significantly, while both **AS1411-5′-TT-Ru** and **AS1411-5′-TTTTT-Ru**, where conjugation is at the 5′ end appear susceptible to degradation, though perhaps to a lesser extent when compared to **AS1411**.

These data may indicate that only **AS1411-5′-TTTTT-Ru** achieves specific uptake in the target cells, while formation of differing G-Quadruplex structures by **AS1411-5′-TT-Ru** and **AS1411-3′-TTT-Ru** (as indicated by their $T_m$ values) may result in only non-specific uptake. Conjugation of the **$RuN_3$** is likely to increase the lipophilicity of the **Ru–AS1411s** and may increase their non-specific uptake. Non-specific uptake and photodynamic effect have been previously reported with **AS1411**.[30]

## Conclusions

In conclusion, we have successfully synthesised an azide functionalized Ruthenium complex **$RuN_3$** and obtained three **Ru–AS1411** by click reaction. A thorough biophysical investigation revealed that the covalently linked Ru complexes did not interfere with G-quadruplex formation, especially when located at the 5′-end of **AS1411**. At a 2 hour incubation timepoint **AS1411-5′-TTTTT-Ru** was selectively photosensitizing towards a cell surface nucleolin expressing cell line (MCF-7), indicating the potential for targeting offered by this system.

Overall, we demonstrate the usefulness of conjugating Ru-based PSs to aptamers to enhance their therapeutic usefulness by conveying specificity to Ru-mediated PDT. Such an approach can readily be expanded to other aptamers by application of this straightforward method described herein and the presence of Ru-based PSs at 5′ termini is not expected to negatively impact the binding efficiency of the resulting aptamer-drug conjugates. A combination of chemically modified aptamers such as XNAs[69–72] that enhance their nuclease stability with potent PSs such as Ru complexes is expected to improve the efficiency of the PDT treatment modality in the near future.

## Experimental

### Synthesis of $RuN_3$

Solvents for reactions were of *pro analysis* (p.a.) grade or distilled prior to use. Ruthenium trichloride *x*-hydrate was provided by $I^2CNS$ (Zurich), 4,7-diphenyl-1,10-phenanthroline, lithium chloride (anhydrous, 99%), and ammonium hexafluorophosphate by Alfa Aesar, sodium azide by Sigma-Aldrich, and 4′-methyl-[2,2′-bipyridine]-4-carboxylic acid by FluoroChem.

### Instrumentation and methods

Amber glass or clear glassware wrapped in tin foil was used when protection from light was necessary. Reactions were carried out under $N_2$ and monitored for completion by HPLC or thin-layer chromatography. Column chromatography: Merck silica gel 60 (40–63 μm) with the indicated solvent system. HPLC: 2× Agilent G1361 1260 Prep Pump system with Agilent G7115A 1260 DAD WR Detector equipped with an Agilent Pursuit XRs 5C18 (Analytic: 100 Å, C18 5 μm 250 × 4.6 mm) Column. The solvents (HPLC grade) were millipore water (0.1% trifluoroacetic acid (TFA)), solvent A) and acetonitrile (MeCN) (0.1% TFA, solvent B). The HPLC gradients used are as follow (S1): 0–3 min: isocratic 95% A (5% B); 3–17 min: linear gradient from 95% A (5% B) to 0% A (100% B); 17–23 min: isocratic 0% A (100% B), 23–25 min: linear gradient from 0% A (100% B) to 95% A (5% B). The flow rate was 1 ml $min^{-1}$. Detection was performed at 215 nm, 250 nm, 350 nm, 450 nm, 550 nm and 650 nm with a slit of 4 nm. IR spectra: spectrumTwo FT-IR Spectrometer (PerkinElmer) equipped with a Specac Golden GateTM ATR (attenuated total reflection) accessory; applied as neat samples; $1/\lambda$ in $cm^{-1}$. NMR-data: deuterated NMR solvents were obtained from Eurisotop (France). $^1H$ NMR spectra in $CD_3OD$ or $CD_3CN$; BrukerAV-400 (400 MHz); $\delta$ in ppm relative to solvent. ($CD_3OD$ (p, 3.31 ppm) and $CD_3CN$ (p, 1.94 ppm)), J in Hz. $^{13}C$ NMR spectra in $CD_3OD$ or $CD_3CN$; Bruker AV-400 (100.6 MHz); $\delta$ in ppm rel. to solv. (($CD_3OD$ (49.00 ppm) and

$CD_3CN$ (118.26 ppm)); multiplicities from DEPT-135 and DEPT-90 experiments. $^{19}F$ NMR spectra in $CD_3OD$ or $CD_3CN$. electrospray ionization mass spectrometry (ESI-MS): experiments were carried out using an LTQ-Orbitrap XL from Thermo Scientific (Thermo Fisher Scientific, Courtaboeuf, France) and operated in positive ionization mode, with a spray voltage of 3.6 kV. No sheath and auxiliary gas were used. Applied voltages were 40 and 100 V for the ion transfer capillary and the tube lens, respectively. The ion transfer capillary was held at 275 °C. Detection was achieved in the Orbitrap with a resolution set to 100.000 (at *m*/*z* 400) and a *m*/*z* range between 150–2000 in profile mode. Spectrum was analyzed using the acquisition software XCalibur 2.1 (Thermo Fisher Scientific, Courtaboeuf, France). The automatic gain control (AGC) allowed the accumulation of up to $21 \times 10^5$ ions for FTMS scans, maximum injection time was set to 300 ms and 1 μscan was acquired. 10 μl was injecting using a Thermo Finnigan Surveyor HPLC system (Thermo Fisher Scientific, Courtaboeuf, France) with a continuous infusion of methanol (MeOH) at 100 μl $min^{-1}$.

### $[Ru(dmso)_4Cl_2]$

**$[Ru(dmso)_4Cl_2]$** was synthesized by adapting a given procedure.[46] Ruthenium(III)-trichloride-*x*-hydrate (9.83 g, 37.6 mmol, assuming $x = 3$) was suspended in EtOH (125 ml, dry) and heated to reflux for 3 h, while a color change from dark brown to dark green was observed. The mixture was filtrated and the solv. was reduced *in vacuo* to afford a deep green paste. The residue was suspended in DMSO (20 ml, dry) and refluxed for 2 h. The heating bath was turned off, and the mixture was left cooling slowly to r.t. in the oil bath while slowly stirring. Cold acetone (200 ml, dry) was added while stirring and the mixture was left overnight at −25 °C for crystallization before filtration. The solid residue was washed several times with acetone to afford **$[Ru(dmso)_4Cl_2]$** as yellow solid (15.5 g, 31.9 mmol, 85%). Spectroscopic data ($^1H$ NMR) were in agreement with the literature.[46] $^1H$ NMR (400 MHz, $D_2O$) $\delta$ 3.58–3.31 (m, 18H), 2.71 (s, 6H). $^{13}C$ NMR (101 MHz, $D_2O$) $\delta$ 46.73, 46.51, 45.70, 45.11, 44.67, 44.32, 38.67.

### $[RuBphen_2Cl_2]$

**$[RuBphen_2Cl_2]$** was synthesized by adapting a given procedure.[73] A mixture of **$[Ru(dmso)_2Cl_2]$** (3.48 g, 7.17 mmol), 4,7-diphenyl-1,10-phenanthroline (Bphen, 5.00 g, 15.0 mmol) and LiCl (2.13 g, 50.3 mmol) was dissolved in DMF (150 ml) and refluxed for 24 h. After cooling to r.t., the solvent was reduced *in vacuo* and acetone (500 ml) was slowly added while stirring. The mixture was then stored at −25 °C overnight for crystallization before filtration. The solid residue was washed with water, acetone and $Et_2O$ to afford **$[RuBphen_2Cl_2]$** as a black-purple solid (3.25 g, 3.88 mmol, 72%). Spectroscopic data ($^1$HNMR) were in agreement with the literature.[73] $^1H$ NMR (400 MHz, $CD_2Cl_2$) $\delta$ 10.55 (s, 2H), 8.50 (d, $J$ = 5.5 Hz, 1H), 8.15 (s, 1H), 8.09 (s, 1H), 8.07 (s, 1H), 7.96 (s, 2H), 7.94 (t, $J$ = 2.8 Hz, 3H), 7.92 (s, 1H), 7.73 (s, 1H), 7.69 (d, $J$ = 6.9 Hz, 3H), 7.63–7.47 (m, 7H), 7.46–7.34 (m, 7H), 7.12 (d, $J$ = 5.6 Hz, 2H). $^{13}C$ NMR (101 MHz, $CD_2Cl_2$) $\delta$ 154.89, 153.04, 152.57, 151.49, 150.88, 149.67, 146.37, 144.96, 137.08, 130.63, 130.18, 129.52, 129.40, 126.10, 125.85, 125.63, 124.90. HPLC: S1 $T_R$ = 7.542 min.

### $N_3EtNH_2$

**$N_3EtNH_2$** was synthesized following a previously published method.[74] $NaN_3$ (2.55 g, 39.2 mmol) was added to a solution of 2-chloroethanamine hydrochloride (1.5 g, 12.9 mmol) in $H_2O$ (10 ml). The resulting mixture was heated with stirring at 80 °C overnight before the reaction was quenched by addition of aqueous KOH (dropwise until a pH of around 12). Following extraction by diethyl ether (3 × 20 ml) and washing with brine (20 ml) the organic layers were combined and dried with anhydrous $MgSO_4$. The solvent was removed carefully *in vacuo* (**$N_3EtNH_2$** is volatile) to give **$N_3EtNH_2$** as a colourless oil (1.54 g, 82%). $^1H$ NMR (400 MHz, MeOD) $\delta$ 3.38 (t, 2H, $J$ = 5.94 Hz), $\delta$ 2.77 (m, 2H).

### $bpyN_3$

The compound *N*-(2-azidoethyl)-4′-methyl-[2,2′-bipyridine]-4-carboxamide (**$bpyN_3$**) was synthesized by suspending 4′-methyl-[2,2′-bipyridine]-4-carboxylic acid (85.70 mg, 0.40 mmol), EDCI-HCl (82.4 mg, 0.43 mmol), NHS (49.10 mg, 0.43 mmol) and in $CH_2Cl_2$ (20 ml). After addition of DIPEA (72.0 μl, 0.45 mmol), the solution is getting clear while left stirring for 30 min. **$N_3EtNH_2$** (90 μl, 0.45 mmol) was added and the mixture was left stirring overnight. The solv. was removed *in vacuo* and the crude residue was purified on alumina (20 : 1 $CH_2Cl_2$/$^i$PrOH) to deliver a colourless oil. After washing with pentane, spontaneous induced crystallization delivered **$bpyN_3$** as a colorless solid (63.2 mg, 0.224 mmol, 56%). $^1H$ NMR (400 MHz, methanol-$d_4$) $\delta$ 8.79 (d, $J$ = 5.3 Hz, 1H *arom.*), 8.68 (s, 1H *arom.*), 8.53 (d, $J$ = 5.1 Hz, 1H *arom.*), 8.22 (s, 1H *arom.*), 7.82–7.68 (m, 1H *arom.*), 7.32 (d, $J$ = 5.0 Hz, 1H *arom.*), 3.62 (t, $J$ = 5.8 Hz, 2H), 3.55 (d, $J$ = 5.8 Hz, 2H), 2.48 (s, 3H).

### $RuN_3$

The complex $[Ru(Bphen)_2(bpyN_3)][PF_6]_2$ (**$RuN_3$**) was synthesized by adapting a given procedure.[49] **$[Ru(Bphen)_2Cl_2]$** (69 mg, 82 μmol) and **$bpyN_3$** (31 mg, 0.108 mmol) were suspended in a water/MeOH mixture (1 : 1, 20 ml, degassed) and refluxed for 15 h resulting in a deep red solution The solution was cooled to r.t. and a few drops of saturated $NH_4PF_6$ solution (sat.) were added while stirring to form a red precipitate. After filtration, the crude solid was purified by column chromatography on silica 60 using a system of MeCN-$KNO_{3aq.}$ (20 : 1, 0.24 M). The product-containing phases were combined and the solv.s were removed *in vacuo*. The redish residue was dissolved in MeOH and a few drops of saturated $NH_4PF_6$ solution and water were added while stirring, to afford a clear solution with a red precipitate. Filtration delivered complex **$RuN_3$** as a red solid (70 mg, 52 μmol, 64%). IR ($cm^{-1}$): 2020w, 1890s, 1620w, 1550w, 1420w, 1310w, 1220w, 1020w, 1100m, 1030w, 830s, 770s, 730m, 700m. $^1H$ NMR (400 MHz, $CD_3CN$) $\delta$ 9.85 (dd, $J$ = 16.9, 5.7 Hz, 1H), 8.89 (d, $J$ = 1.4 Hz, 1H *arom.*), 8.61 (s, 1H *arom.*), 8.29 (dd, $J$ = 18.9, 5.5 Hz, 2H *arom.*), 8.20 (dd, $J$ = 12.0, 9.5 Hz, 2H *arom.*), 8.19 (s, 2H), 8.10 (dd, $J$ = 5.5, 2.8 Hz, 2H *arom.*), 8.01 (dd, $J$ = 5.9,

0.6 Hz, 1H *arom.*), 7.75 (t, $J$ = 5.5 Hz, 2H *arom.*), 7.72–7.55 (m, 24H *arom.*), 7.26 (ddd, $J$ = 5.8, 1.8, 0.8 Hz, 1H *arom.*), 3.61 (q, $J$ = 5.3 Hz, 2H), 3.53 (t, $J$ = 5.7 Hz, 2H), 2.59 (s, 3H). $^{13}$C NMR (101 MHz, $CD_3CN$) $\delta$ 153.16, 153.02, 152.34, 150.12, 143.13, 136.69, 136.63, 130.81, 130.75, 130.69, 130.65, 130.15, 130.11, 129.99, 127.05, 126.49, 125.13, 122.55, 51.03, 40.30, 21.28. $^{19}$F NMR (376 MHz, $CD_3CN$) $\delta$ −72.74 (d, $J$ = 707.1 Hz, $PF_6$). HR-MS ($ESI^+$): $m/z$ 524.1447 $[M - 2(PF_6)]^{2+}$ (calculated: 524.1453). HPLC: S1 $T_R$ = 16.271 min.

### Click reactions

Oligonucleotides **T1**, **T2** and **T5** were purchased from Microsynth AG, oligonucleotides **T3** and **T4** were ordered from Integrated DNA Technologies and were stored at 1 mM in $H_2O$. **RuN$_3$** was stored at 5 mM in DMF, Sodium ascorbate was made fresh at 50 mM in $H_2O$, $CuSO_4$ was stored at 5 mM in $H_2O$, TBTA was stored at 10 mM in DMSO. All solutions were thoroughly degassed by argon bubbling prior and post mixing of appropriate quantities of stock solutions. The reactions were performed in Eppendorf tubes at 30 °C with gentle shaking for 2 hours. The Monarch® PCR & DNA Cleanup Kit was used to desalt the reactions before HPLC purification. The quantities of reagents used is specified in Table 5. Confirmation of product formation was obtained by LCMS ($m/z$ found: 10082.7427, 10994.8808 and 10560.8611 for **AS1411-5′-TT-Ru**, **AS1411-5′-TTTTT-Ru** and **AS1411-3′-TTT-Ru** respectively).

### HPLC

HPLC purification was performed using an Äkta™ pure system (GE Healthcare) equipped with Kinetex® semi preparative Reversed Phase C18 column (5 μm, 250 × 10.0 mm). Buffer A: 20 mM Triethylammonium acetate (TEAA) buffer; buffer B: 30% 20 mM TEAA/70% Acetonitrile. A flow rate of 1.5 ml min$^{-1}$ was used with UV/Vis detection at 280 and 430 nm.

### Spectroscopic measurements

The absorption spectra of the sample was measured with a SpectraMax M2 Spectrometer (Molecular Devices). For measurement of the emission, the sample was irradiated at 450 nm with a NT342B Nd-YAG pumped optical parametric oscillator (Ekspla). The emission was focused at right angle to the excitation pathway and directed to a Princeton Instruments Acton SP-2300i monochromator. The signal was detected with a XPI-Max 4 CCD camera (Princeton Instruments).

Table 5 Ratios of reagents used in click reactions

| | Original[a] (μl) | Revised (μl) |
|---|---|---|
| Oligonucleotide (1 mM) | 100 | 100 |
| **RuN$_3$** (5 mM) | 100 | 100 |
| $CuSO_4$ (10 mM) | 100 | 10 |
| TBTA (10 mM) | | 20 |
| Na ascorbate (50 mM) | 100 | 100 |
| Tris buffer 10× | 40 | 34 |
| Acetonitrile | 10 | 10 |

[a] Not recommended.

### LC-MS

LC-MS analyses were performed on a Q exactive mass spectrometer (Thermo Fisher Scientific) equipped with an electrospray ionisation source (H-ESI II Probe) coupled with an Ultimate 3000 RS HPLC (Thermo Fisher Scientific). Compounds were injected onto a ThermoFisher Hypersil Gold aQ chromatography column (100 mm × 2.1 mm, 1.9 μm particle size) heated at 30 °C. The flow rate was set at 0.3 ml min$^{-1}$ and the mobile phase consisted of (A) water + 0.1% formic acid and (B) acetonitrile + 0.1% formic acid. The gradient used was: 5% B during 0–3 minutes then 5% to 100% B linear during 3–8 minutes. Ions were analysed in negative ion mode. MS resolution was 70 000 with an AGC target of 1$^e$6 and a maximum injection time of 240 ms. Multicharged ions were processed using Xtract software. A UV detector set at 270 nm was also used as a control.

### Luminescence quantum yield

The sample was prepared in an acetonitrile solution with an absorption of 0.1 at 450 nm. The sample was irradiated at 450 nm with a NT342B Nd-YAG pumped optical parametric oscillator (Ekspla). The emission was focused at right angle to the excitation pathway and directed to a Princeton Instruments Acton SP-2300i monochromator. The signal was detected with a XPI-Max 4 CCD camera (Princeton Instruments). The luminescence quantum yields were determined by comparison with the reference $[Ru(2,2'\text{-bipyridine})_3]Cl_2$ in acetonitrile ($\Phi_{em}$ = 5.9%[56]) applying the following formula:

$$\Phi_{em,sample} = \Phi_{em,reference} \times (F_{reference}/F_{sample}) \times (I_{sample}/I_{reference}) \times (n_{sample}/n_{reference})^2 \quad (1)$$

$$F = 1 - 10^{-A} \quad (2)$$

$\Phi_{em}$ = luminescence quantum yield, $F$ = fraction of light absorbed, $I$ = integrated emission intensities, $n$ = refractive index, $A$ = absorbance of the sample at irradiation wavelength.

### Lifetime

The sample was prepared in an air saturated as well as a degassed acetonitrile solution with an absorption of 0.2 at 450 nm. The sample was irradiated at 450 nm with a NT342B Nd-YAG pumped optical parametric oscillator (Ekspla). The emission was focused at right angle to the excitation pathway and directed to a Princeton Instruments Acton SP-2300i monochromator. The signal was detected with a R928 photomultiplier tube (Hamamatsu).

### Singlet oxygen – direct evaluation

The sample was prepared in an air saturated acetonitrile or $D_2O$ solution with an absorption of 0.2 at 450 nm. The sample was irradiated at 450 nm with a mounted M450LP1 LED (Thorlabs) whose light was focused with aspheric condenser lenses. Using a T-Cube LED Driver (Thorlabs), the intensity of the irradiation was varied and monitored with an optical power and energy meter. The emission was focused at right angle to the excitation pathway and directed to a Princeton Instruments Acton

SP-2300i monochromator. To cut off light at wavelengths shorter than 850 nm, a longpass glass filter was placed in front of the monochromator entrance slit. The signal was detected with an EO-817L IR-sensitive liquid nitrogen cooled germanium diode detector (North Coast Scientific Corp.). The luminescence signal, centered at 1270 nm, was measured from 1100 to 1400 nm. The obtained data was analyzed upon plotting the integrated luminescence peaks against the percentage of the irradiation intensity. The slope of the linear regression was calculated and compared with the reference Rose Bengal ($\Phi$ = 76%[75]). The absorption of the sample was corrected with an absorption correction factor. The singlet oxygen quantum yields were calculated using the following formula:

$$\Phi_{\text{sample}} = \Phi_{\text{reference}} \times (S_{\text{sample}}/S_{\text{reference}}) \times (I_{\text{reference}}/I_{\text{sample}}) \quad (3)$$

$$I = I_0 \times (1 - 10^{-A}) \quad (4)$$

$\Phi$ = singlet oxygen quantum yield, $S$ = slope of the linear regression of the plot of the areas of the singlet oxygen luminescence peaks against the irradiation intensity, $I$ = absorption correction factor, $I_0$ = light intensity of the irradiation source, $A$ = absorption of the sample at irradiation wavelength.

### Singlet oxygen – indirect evaluation

Measurement in acetonitrile: the sample was prepared in an air-saturated acetonitrile solution with an absorption of 0.2 at the irradiation wavelength, *N*,*N*-dimethyl-4-nitrosoaniline aniline (RNO, 24 μM) and imidazole (12 mM). Measurement in PBS buffer: The sample was prepared in an air-saturated PBS solution containing the complex with an absorption of 0.2 at the irradiation wavelength, *N*,*N*-dimethyl-4-nitrosoaniline aniline (RNO, 20 μM) and histidine (10 mM). The samples were irradiated for various time points with an Atlas Photonics LUMOS BIO irradiator. The absorption of the samples was constantly monitored with a SpectraMax M2 Microplate Reader (Molecular Devices). The difference in absorption ($A_0 - A$) at 420 nm for the measurement in acetonitrile or at 440 nm for the measurement in PBS was determined. The difference in absorption was then plotted against the irradiation times and the slope of the linear regression calculated. The absorption of the sample was corrected with an absorption correction factor. The singlet oxygen quantum yields were calculated using the same formulas as used for the direct evaluation.

### Gel electrophoresis

Acrylamide/bisacrylamide (29 : 1, 40%) was obtained from Fisher Scientific. Visualization of PAGE gels was performed by fluorescence imaging using a Typhoon Trio phosphorimager with the ImageQuant software from GE Healthcare. Samples were loaded in blue loading dye (70% formamide, EDTA 50 mM, 0.1% bromophenol blue, 0.1% xylene cyanol, $H_2O$).

### CD spectroscopy

Circular dichroism experiments were performed on a Aviv 215 spectropolarimeter at 37 °C. Concentration of **AS1411** and **Ru–AS1411s** was kept constant (10 μM in water) and CD measured using a 1 cm pathlength cuvette. Stock salt solutions (1 M KCl and NaCl) were used. CD spectra were recorded at the Molecular Biophysics platform at Institut Pasteur.

### Thermal difference spectra

TDS were performed on an Agilent Cary UV-Vis Compact Peltier machine in 60 μl volume quartz cuvettes. The UV/Vis absorption spectra of concentrations of around 3 μM were measured between 335 nm and 220 nm at 20 °C and 90 °C. The TDS was generated by subtracting the spectra at 20 °C from those at 90 °C following a previously published protocol.[65]

### Cell culture experiments

Cells lines were treated in appropriate cell culture media of DMEM (Gibco, LifeTechnologies, USA) supplemented with 10% foetal calf serum (FCS) for the HT29 and MCF-7 cell lines (Gibco) and DMEM/F-12 (Gibco) supplemented with 10% foetal calf serum (Gibco) for the RPE-1 cell line. All media was also supplemented with 100 U $ml^{-1}$ penicillin–streptomycin mixture (Gibco). Cells were incubated at 37 °C in 5% $CO_2$. Cells were passaged when 80% confluency was reached and used within 15 passages from initial purchase. **Ru–AS1411s** were stored at 20 μM in sterile 50 mM KCl. **$RuN_3$** was stored in DMSO at 10 mM.

### Cytotoxicity experiments

96 well dishes were seeded with MCF-7 cells (6000 cells per well) or RPE-1 cells (4000 cells per well) and incubated overnight. Cell media was replaced with treatment solutions prepared to the concentrations specified and incubated for 2 or 4 hours. Concentrations of additional KCl (5 mM) and DMSO (0.01%) were kept constant across treatments. Following the incubation, wells were washed (2 × PBS) and the media replaced (100 μl) before either being treated with light ($\lambda_{exc}$ = 480 nm, 3.21 J $cm^{-2}$, 10 min) or kept in the dark. After 48 h incubation the cells were treated with resazurin (0.2 mg $mL^{-1}$ final concentration in appropriate media) and incubated a further 4 h. The plates were read by fluorescence plate reader SpectraMax M5 micro plate reader ($\lambda_{ex}$, 540 nm; $\lambda_{em}$, 590 nm).

### Confocal microscopy

Sterilized 12 mm Menzel–Gläser coverslips were added to 6 well dishes (3 coverslips per well) and seeded with cells ($2 \times 10^5$ cells per well for HT-29 and MCF-7 cell lines and $1.5 \times 10^5$ for RPE-1) and incubated overnight. For **Ru–AS1411s** imaging, coverslips were transferred to separate wells in a 12-well dish and treatment solutions added. Following a 2 hour time point the wells were washed (3 × PBS) and treated with paraformaldehyde (4% in PBS, 15 min) before being washed (3 × PBS) and mounted to microscope slides (Prolong Glass Antifade Mountant). For anti-nucleolin staining coverslips were transferred to separate wells in a 12-well dish and incubated with Nucblue (2 drops $ml^{-1}$ in media, 20 min) before being washed (3 × PBS) and treated with paraformaldehyde (4% in PBS, 15 min) before being washed again (3 × PBS). Blocking solution was added (0.2% BSA, 0,05%

Saponin in PBS) for 15 min at RT. The primary antibody anti-nucleolin (ZN004, Thermofisher) was added (5 μg $ml^{-1}$, 1 h) before the cover slips were washed (3 × 0.2% BSA, 0.05% Saponin in PBS) and the secondary antibody added Alexa 488 conjugated secondary antibodies (Jackson ImmunoResearch Laboratory, 1 : 400 dilution, 30 min). The coverslips were then mounted to microscope slides (Prolong Glass Antifade Mountant). The slides were then imaged. For the **Ru–AS1411s** $\lambda_{exc}$ = 405 nm and $\lambda_{em}$ = 600–750 nm. The microscope DAPI imaging settings were used for Nucblue and $\lambda_{exc}$ = 488 nm, $\lambda_{em}$ = 510–540 nm used to image the secondary antibody. Images were recorded at the Cellular and Molecular Imaging Technical Platform, INSERM-UMS025–CNRSUMS3612, Faculty of Pharmacy of Paris, Paris Descartes University, Paris, France.

### $T_m$ measurements

The melting experiments were performed on an Agilent Cary UV-Vis Compact 3500 Peltier machine in 60 μl volume quartz cuvettes. **AS1411** samples were prepared in 0.1 M KCl to yield a solution with $OD_{295}$ between 0.3 and 0.6. Paraffin oil (100 μl) was added. A control cell (0.1 M KCl) was prepared into which the temperature probe was placed. The Tm values were measured with a total of three heating and cooling ramps each (1 °C $minute^{-1}$) with data processed from the heating ramps.

### Media stability tests

Samples of all three **Ru–AS1411s** (20 pmol each, 1 μL from 20 μM sample in 50 mM KCl) were incubated in cell culture medium (DMEM with 10% FCS, 10 μl each) and incubated for the stated time at 37 °C. Blue loading dye was added (10 μl) and sampled heated (95 °C, 5 min) before being loaded on PAGE gel.

## Conflicts of interest

The authors declare no competing financial interests.

## Acknowledgements

We thank Dr Philippe Goldner for access to state-of-the-art laser apparatus. We thank financial support from the Technology Transfer and Industrial Partnership Department (DARRI) of Institut Pasteur (grant INNOV 17-19) and the Joe W. and Dorothy Doresett Brown Foundation (exploratory and advanced grants). This work was financially supported by an ERC Consolidator Grant PhotoMedMet to G. G. (GA 681679), has received support under the program "Investissements d' Avenir" launched by the French Government and implemented by the ANR with the reference ANR-10-IDEX-0001-02 PSL (G. G.). L. K. M. thanks the ARC Foundation for cancer research for a postdoctoral Research Fellowship (grant number: S-FB18006). A. G also thanks the ARC Foundation for cancer research for a postdoctoral Research Fellowship. The authors acknowledge a DIM1Health 2019 grant from the Région Ile de France to the project EpiK (coordinated by P. B. Arimondo) for the LCMS equipment. M. F. gratefully acknowledges a fellowship from the doctoral school MTCI, Université de Paris.

## References

1 J. Karges, F. Heinemann, M. Jakubaszek, F. Maschietto, C. Subecz, M. Dotou, R. Vinck, O. Blacque, M. Tharaud, B. Goud, E. Viñuelas-Zahinos, B. Spingler, I. Ciofini and G. Gasser, *J. Am. Chem. Soc.*, 2020, **142**, 6578–6587.
2 S. Monro, K. L. Colón, H. Yin, J. Roque III, P. Konda, S. Gujar, R. P. Thummel, L. Lilge, C. G. Cameron and S. A. McFarland, *Chem. Rev.*, 2018, **119**, 797–828.
3 L. K. McKenzie, H. E. Bryant and J. A. Weinstein, *Coord. Chem. Rev.*, 2019, **379**, 2–29.
4 F. Heinemann, J. Karges and G. Gasser, *Acc. Chem. Res.*, 2017, **50**, 2727–2736.
5 J. D. Knoll and C. Turro, *Coord. Chem. Rev.*, 2015, **282**, 110–126.
6 C. Mari, V. Pierroz, S. Ferrari and G. Gasser, *Chem. Sci.*, 2015, **6**, 2660–2686.
7 S. A. McFarland, A. Mandel, R. Dumoulin-White and G. Gasser, *Curr. Opin. Chem. Biol.*, 2020, **56**, 23–27.
8 M. G. Walker, P. J. Jarman, M. R. Gill, X. Tian, H. Ahmad, P. A. Reddy, L. McKenzie, J. A. Weinstein, A. J. Meijer and G. Battaglia, *Chem. – Eur. J.*, 2016, **22**, 5996–6000.
9 F. E. Poynton, S. A. Bright, S. Blasco, D. C. Williams, J. M. Kelly and T. Gunnlaugsson, *Chem. Soc. Rev.*, 2017, **46**, 7706–7756.
10 L. Zeng, P. Gupta, Y. Chen, E. Wang, L. Ji, H. Chao and Z.-S. Chen, *Chem. Soc. Rev.*, 2017, **46**, 5771–5804.
11 C. S. Burke, A. Byrne and T. E. Keyes, *J. Am. Chem. Soc.*, 2018, **140**, 6945–6955.
12 P. S. Felder, S. Keller and G. Gasser, *Adv. Therapeutics*, 2020, **3**, 1900139.
13 M. Jakubaszek, B. Goud, S. Ferrari and G. Gasser, *Chem. Commun.*, 2018, **54**, 13040–13059.
14 S. Chakrabortty, B. K. Agrawalla, A. Stumper, N. M. Vegi, S. Fischer, C. Reichardt, M. Kögler, B. Dietzek, M. Feuring-Buske and C. Buske, *J. Am. Chem. Soc.*, 2017, **139**, 2512–2519.
15 D. Cullinane, K. S. Gkika, A. Byrne and T. E. Keyes, *J. Inorg. Biochem.*, 2020, **207**, 111032.
16 A. Martin, A. Byrne, C. S. Burke, R. J. Forster and T. E. Keyes, *J. Am. Chem. Soc.*, 2014, **136**, 15300–15309.
17 J. Karges, M. Jakubaszek, C. Mari, K. Zarschler, B. Goud, H. Stephan and G. Gasser, *ChemBioChem*, 2020, **21**, 531–542.
18 W. Sun, S. Li, B. Häupler, J. Liu, S. Jin, W. Steffen, U. S. Schubert, H. J. Butt, X. J. Liang and S. Wu, *Adv. Mater.*, 2017, **29**, 1603702.
19 N. Soliman, L. K. McKenzie, J. Karges, E. Bertrand, M. Tharaud, M. Jakubaszek, V. Guérineau, B. Goud, M. Hollenstein and G. Gasser, *Chem. Sci.*, 2020, **11**, 2657–2663.
20 E. Villemin, Y. C. Ong, C. M. Thomas and G. Gasser, *Nat. Rev. Chem.*, 2019, **3**, 261–282.
21 Y. Ellahioui, M. Patra, C. Mari, R. Kaabi, J. Karges, G. Gasser and S. Gómez-Ruiz, *Dalton Trans.*, 2019, **48**, 5940–5951.
22 J. Karges, J. Li, L. Zeng, H. Chao and G. Gasser, *ACS Appl. Mater. Interfaces*, 2020, **12**, 54433–54444.

23 J. Yan, T. Gao, Z. Lu, J. Yin, Y. Zhang and R. Pei, *ACS Appl. Mater. Interfaces*, 2021, **13**, 27749–27773.
24 P. Röthlisberger and M. Hollenstein, *Adv. Drug Delivery Rev.*, 2018, **134**, 3–21.
25 L. K. McKenzie, R. El-Khoury, J. D. Thorpe, M. J. Damha and M. Hollenstein, *Chem. Soc. Rev.*, 2021, **50**, 5126–5164.
26 L. Li, S. Xu, H. Yan, X. Li, H. S. Yazd, X. Li, T. Huang, C. Cui, J. Jiang and W. Tan, *Angew. Chem., Int. Ed.*, 2021, **60**, 2221–2231.
27 P. J. Bates, D. A. Laber, D. M. Miller, S. D. Thomas and J. O. Trent, *Exp. Mol. Pathol.*, 2009, **86**, 151–164.
28 C. M. Berger, X. Gaume and P. Bouvet, *Biochimie*, 2015, **113**, 78–85.
29 C. R. Ireson and L. R. Kelland, *Mol. Cancer Ther.*, 2006, **5**, 2957–2962.
30 Y.-A. Shieh, S.-J. Yang, M.-F. Wei and M.-J. Shieh, *ACS Nano*, 2010, **4**, 1433–1442.
31 Q. Liu, L. Xu, X. Zhang, N. Li, J. Zheng, M. Guan, X. Fang, C. Wang and C. Shu, *Chem. – Asian J.*, 2013, **8**, 2370–2376.
32 J. Ai, Y. Xu, B. Lou, D. Li and E. Wang, *Talanta*, 2014, **118**, 54–60.
33 J. Kim, W. Park, D. Kim, E. S. Lee, D. H. Lee, S. Jeong, J. M. Park and K. Na, *Adv. Funct. Mater.*, 2019, **29**, 1900084.
34 Y. Yang, J. He, W. Zhu, X. Pan, H. S. Yazd, C. Cui, L. Yang, X. Li, L. Li and L. Cheng, *Theranostics*, 2020, **10**, 4030.
35 X. Zhu, H. Zhou, Y. Liu, Y. Wen, C. Wei, Q. Yu and J. Liu, *Acta Biomater.*, 2018, **82**, 143–157.
36 L. Xu, X. Chen, J. Wu, J. Wang, L. Ji and H. Chao, *Chem. – Eur. J.*, 2015, **21**, 4008–4020.
37 D. Sun, Y. Liu, D. Liu, R. Zhang, X. Yang and J. Liu, *Chem. – Eur. J.*, 2012, **18**, 4285–4295.
38 G.-L. Liao, X. Chen, L.-N. Ji and H. Chao, *Chem. Commun.*, 2012, **48**, 10781–10783.
39 E. Wachter, D. Moyá, S. Parkin and E. C. Glazer, *Chem. – Eur. J.*, 2016, **22**, 550–559.
40 G. Piraux, L. Bar, M. Abraham, T. Lavergne, H. Jamet, J. Dejeu, L. Marcélis, E. Defrancq and B. Elias, *Chem. – Eur. J.*, 2017, **23**, 11872–11880.
41 L. Xu, D. Zhang, J. Huang, M. Deng, M. Zhang and X. Zhou, *Chem. Commun.*, 2010, **46**, 743–745.
42 K. McQuaid, H. Abell, S. P. Gurung, D. R. Allan, G. Winter, T. Sorensen, D. J. Cardin, J. A. Brazier, C. J. Cardin and J. P. Hall, *Angew. Chem., Int. Ed.*, 2019, **58**, 9881–9885.
43 Q. Yu, Y. Liu, C. Wang, D. Sun, X. Yang, Y. Liu and J. Liu, *PLoS One*, 2012, **7**, e50902.
44 J. Weynand, A. Diman, M. Abraham, L. Marcélis, H. Jamet, A. Decottignies, J. Dejeu, E. Defrancq and B. Elias, *Chem. – Eur. J.*, 2018, **24**, 19216–19227.
45 N. Zabarska, A. Stumper and S. Rau, *Dalton Trans.*, 2016, **45**, 2338–2351.
46 I. Brastos, E. Alessio, M. E. Ringenberg and T. B. Rauchfuss, *Inorg. Synth.*, 2010, **35**, 148–163.
47 R. Caspar, C. Cordier, J. B. Waern, C. Guyard-Duhayon, M. Gruselle, P. Le Floch and H. Amouri, *Inorg. Chem.*, 2006, **45**, 4071–4078.
48 C. A. Panetta, H. J. Kumpaty, N. E. Heimer, M. C. Leavy and C. L. Hussey, *J. Org. Chem.*, 1999, **64**, 1015–1021.
49 J. Karges, F. Heinemann, F. Maschietto, M. Patra, O. Blacque, I. Ciofini, B. Spingler and G. Gasser, *Bioorg. Med. Chem.*, 2019, **27**, 2666–2675.
50 J. Iley and R. Tolando, *J. Chem. Soc., Perkin Trans. 2*, 2000, 2328–2336, DOI: 10.1039/b001756f.
51 V. G. Correia, J. C. Abreu, C. A. Barata and L. H. Andrade, *Org. Lett.*, 2017, **19**, 1060–1063.
52 Q. Sun, Z. Kang, L. Xue, Y. Shang, Z. Su, H. Sun, Q. Ping, R. Mo and C. Zhang, *J. Am. Chem. Soc.*, 2015, **137**, 6000–6010.
53 G. Lemercier, M. Four and S. Chevreux, *Coord. Chem. Rev.*, 2018, **368**, 1–12.
54 J. Karges, O. Blacque, P. Goldner, H. Chao and G. Gasser, *Eur. J. Inorg. Chem.*, 2019, 3704–3712.
55 J. Karges, D. Díaz-García, S. Prashar, S. Gómez-Ruiz and G. Gasser, *ACS Appl. Bio Mater.*, 2021, **4**, 4394–4405.
56 K. Nakamaru, *Bull. Chem. Soc. Jpn.*, 1982, **55**, 1639–1640.
57 J. Karges, S. Kuang, F. Maschietto, O. Blacque, I. Ciofini, H. Chao and G. Gasser, *Nat. Commun.*, 2020, **11**, 1–13.
58 Y. W. Cheung, P. Röthlisberger, A. E. Mechaly, P. Weber, F. Levi-Acobas, Y. Lo, A. W. C. Wong, A. B. Kinghorn, A. Haouz, G. P. Savage, M. Hollenstein and J. A. Tanner, *Proc. Natl. Acad. Sci. U. S. A.*, 2020, **117**, 16790–16798.
59 N. Z. Fantoni, A. H. El-Sagheer and T. Brown, *Chem. Rev.*, 2021, **121**(12), 7122–7154.
60 D. Ganz, D. Harijan and H.-A. Wagenknecht, *RSC Chem. Biol.*, 2020, **1**, 86–97.
61 S. Mack, M. F. Fouz, S. K. Dey and S. R. Das, *Curr. Protocols Chem. Biol.*, 2016, **8**, 83–95.
62 I. Kejnovska, D. Renciuk, J. Palacky and M. Vorlickova, *Methods Mol. Biol.*, 2019, **2035**, 25–44.
63 M. M. Dailey, M. C. Miller, P. J. Bates, A. N. Lane and J. O. Trent, *Nucleic Acids Res.*, 2010, **38**, 4877–4888.
64 Z. Bagheri, B. Ranjbar, H. Latifi, M. I. Zibaii, T. T. Moghadam and A. Azizi, *Int. J. Biol. Macromol.*, 2015, **72**, 806–811.
65 J. Carvalho, A. Paiva, M. P. C. Campello, A. Paulo, J.-L. Mergny, G. F. Salgado, J. A. Queiroz and C. Cruz, *Sci. Rep.*, 2019, **9**, 1–12.
66 G. R. Abel Jr, Z. A. Calabrese, J. Ayco, J. E. Hein and T. Ye, *Bioconjugate Chem.*, 2016, **27**, 698–704.
67 K. Liu, P. K. Lat, H.-Z. Yu and D. Sen, *Nucleic Acids Res.*, 2020, **48**, 7356–7370.
68 Y. Jing, M. Cai, L. Zhou, J. Jiang, J. Gao and H. Wang, *Talanta*, 2020, **217**, 121037.
69 M. R. Dunn, C. M. McCloskey, P. Buckley, K. Rhea and J. C. Chaput, *J. Am. Chem. Soc.*, 2020, **142**, 7721–7724.
70 E. Eremeeva, A. Fikatas, L. Margamuljana, M. Abramov, D. Schols, E. Groaz and P. Herdewijn, *Nucleic Acids Res.*, 2019, **47**, 4927–4939.
71 K. M. Rose, I. A. Ferreira-Bravo, M. Li, R. Craigie, M. A. Ditzler, P. Holliger and J. J. DeStefano, *ACS Chem. Biol.*, 2019, **14**, 2166–2175.
72 A. E. Rangel, Z. Chen, T. M. Ayele and J. M. Heemstra, *Nucleic Acids Res.*, 2018, **46**, 8057–8068.

73 A. Notaro, M. Jakubaszek, N. Rotthowe, F. Maschietto, R. Vinck, P. S. Felder, B. Goud, M. Tharaud, I. Ciofini, F. Bedioui, R. F. Winter and G. Gasser, *J. Am. Chem. Soc.*, 2020, **142**, 6066–6084.
74 J. Dash, Z. A. Waller, G. D. Pantoş and S. Balasubramanian, *Chem. – Eur. J.*, 2011, **17**, 4571–4581.
75 I. E. Kochevar and R. W. Redmond, *Methods Enzymol.*, 2000, **319**, 20–28.